A&A 483, 137–149 (2008)
DOI: 10.1051/0004-6361:20079075

Astronomy & Astrophysics

X-ray spectral variability in PG 1535+547: the changing look of a "soft X-ray weak" AGN

L. Ballo[1], M. Giustini[2,3], N. Schartel[1], M. Cappi[3], E. Jiménez-Bailón[4], E. Piconcelli[5], M. Santos-Lleó[1], and C. Vignali[2,6]

[1] XMM-Newton Science Operation Centre, ESAC, ESA, PO Box 78, 28691 Villanueva de la Cañada, Madrid, Spain
e-mail: lucia.ballo@sciops.esa.int
[2] Dipartimento di Astronomia, Università degli Studi di Bologna, via Ranzani 1, 40127 Bologna, Italy
[3] Istituto di Astrofisica Spaziale e Fisica cosmica (INAF), via Gobetti 101, 40129 Bologna, Italy
[4] Instituto de Astronomía, Universidad Nacional Autónoma de México, Apartado Postal 70-264, 04510-Mexico DF, México
[5] Osservatorio Astronomico di Roma (INAF), via Frascati 33, 00040 Monteporzio Catone, Roma, Italy
[6] Osservatorio Astronomico di Bologna (INAF), via Ranzani 1, 40127 Bologna, Italy

Received 15 November 2007 / Accepted 18 February 2008

ABSTRACT

Context. PG 1535+547 is a bright Narrow Line Seyfert 1 galaxy, whose high-energy emission shows strong variability both in shape and flux. On the basis of *ROSAT* observations, it is classified as "soft X-ray weak quasi-stellar object (QSO)", a class of objects whose X-ray-to-optical flux ratio is smaller than in typical QSOs. Their X-ray spectra are often characterized by highly-ionized, complex absorbers and/or reflection from the inner accretion disk, and the relative importance of the two is currently debated. Whatever the correct interpretation may be, the presence of such features implies that we are looking at matter located in the innermost regions of these AGN.

Aims. We want to clarify the nature of the X-ray emission of PG 1535+547, and constrain the physical properties of its innermost regions, where this emission originates.

Methods. We present new XMM-Newton observations of PG 1535+547 (90 ks exposure time, January 2006), from which we obtained two spectra European Photon Imaging Camera (EPIC) separated by about one week. We compare these spectra with those from a previous (November 2002) XMM-Newton observation.

Results. These latest observations support the complex and variable nature of the X-ray emission of PG 1535+547. The broadband observed flux increases by a factor ∼2.3 in three years, and then decreases by a factor ∼1.3 in about one week. In the new spectra, strong absorption features at $E < 3$ keV and a complex spectral shape in the iron-line energy range are evident, coupled with a drop in the emission at higher energies. We describe all the different states in a consistent way, assuming either a warm absorber plus a relativistically-blurred ionized reflection, or a two-phase warm absorber partially covering the source with the addition of a scattered component.

Conclusions. The observed variability can be ascribed mostly to warm absorbing gas in the innermost regions of PG 1535+547, which appears to vary in its physical properties on timescales of both years and days. In the blurred reflection scenario, all the analyzed states require a high fraction of reflection from the disk, calling for some mechanisms able to increase the reflection component with respect to the intrinsic continuum. Finally, the strong variability observed in the X-ray band opposed to a more constant emission at optical frequencies, changes the value of the X-ray-to-optical spectral index, implying that PG 1535+547 can not actually be classified as a soft X-ray weak active galactic nucleus (AGN).

Key words. galaxies: active – galaxies: quasars: individual: PG 1535+547 – X-rays: galaxies

1. Introduction

Studying the X-ray emission from active galactic nuclei (AGN) offers the potential to investigate the central engine powering these sources. The fluorescent Fe emission line complex at 6.4–7 keV is an important direct probe of the dense matter around the nuclear region, from the molecular torus and the broad line region (BLR) to the inner-accretion disk, down to a few gravitational radii ($r_g \equiv GM_{BH}/c^2$). In the latter case, intrinsically-narrow emission lines emitted by the accretion disk are predicted to be broadened by Doppler and relativistic effects. Detailed studies of their energy profiles and flux variability could give strong constraints on the geometry and kinematics of the accretion disk in terms of inclination, inner and outer radii of the emitting region and ionization state (e.g., Miller et al. 2006; see Reynolds & Nowak 2003, for a review).

The inner region of AGN houses also "warm" (i.e., partially photoionized, $T \sim 10^5$ K) gas that absorbs the nuclear emission in the X-ray band. This "warm absorber" (Halpern 1984) is often found to be complex and multi-phase, and outflowing with velocities in the range 0.001–0.01 c (e.g., Piconcelli et al. 2004; Ashton et al. 2004; Blustin et al. 2005; McKernan et al. 2007). Recently, more extreme outflow velocities (i.e., up to ∼0.3 c) have been detected in the X-ray spectra of a few dozen AGN (for a review, see Cappi 2006). The knowledge of the properties of warm absorbers such as their location, covering fraction, mass content, and outflow velocity can help us to understand not only the accretion/ejection mode of AGN, but also their impact on the surrounding medium. Constraining the physical properties of ionized gas harbored in the inner regions of AGN and disentangle reflection from absorption contribution are challenges

that can be unfolded only via high energy, temporally resolved spectral analyses.

Linked to both these topics, the origin of the so-called "soft excess", an enhancement of flux seen below 2−3 keV with respect to the extrapolation at low energies of the hard nuclear component, is still a debated point. While the constancy of its "temperature" over a wide range of luminosities and black hole masses seems in contrast with the idea of direct thermal emission from the accretion disk (see e.g. Piconcelli et al. 2005), two different explanations have been proposed (both probably playing a fundamental role in a complex combination, see e.g., Chevallier et al. 2006): photoionized reflection from the inner-accretion disk (Crummy et al. 2006), or absorption from a relativistically outflowing, moderately-ionized medium (Gierliński & Done 2004, 2006; Schurch & Done 2006; Sobolewska & Done 2007).

In previous years, a comparison between optical and X-ray properties of bright sources pointed out the existence of a population of AGN notably faint in soft X-ray relative to their optical fluxes, the so-called "soft X-ray weak quasi-stellar object (QSO)" (Laor et al. 1997). Analyzing the X-ray emission of the Boroson & Green (1992) sample of nearby AGN, Brandt et al. (2000) found that approximately 10% of optically-selected AGN are X-ray weak at soft energies, with an X-ray-to-optical spectral index $\alpha_{ox} \equiv \log(F_{2\,keV}/F_{3000\,Å})/\log(\nu_{2\,keV}/\nu_{3000\,Å}) < -2$. The strong correlation observed between α_{ox} and absorption features in the UV band (mainly the C IV absorption equivalent width) supports the idea of X-ray absorption as the primary cause of their soft X-ray weakness. This makes the X-ray weak AGN an important target to study the ionization structure and the matter distribution of the warm absorbers, whose presence seems to be linked to absorption in the UV band (Brinkmann et al. 2004; Piconcelli et al. 2004). In this case, a sample composed by soft X-ray weak AGN would have a high incidence of X-ray obscured sources, playing an important role, e.g., in the X-ray background synthesis models as well as in unified AGN schemes.

On the other hand, Risaliti et al. (2003) from a "mini-survey" of 18 quasars observed with *Chandra* found a high incidence of intrinsically under-luminous objects, suggesting that they represent a population with a spectral energy distribution (SED) different from that of standard blue quasars. So, a different intrinsic X-ray emission mechanism cannot be completely ruled out. A strong variability of the intrinsic continuum might be another reason for an X-ray weakness at the time of the observation (see, e.g., the case of PG 0844+349; Brinkmann et al. 2003). Recently, Schartel et al. (2007) explained the weak X-ray emission of PG 2112+059 with light bending (Miniutti & Fabian 2004) instead of absorption, suggesting these sources as ideal targets to observe the accretion disk near the central black hole.

In this paper, we present new XMM-Newton data of a soft X-ray weak QSO, PG 1535+547, comparing the results with previous XMM-Newton observations. In our analysis, we assume a cosmology with $\Omega_M = 0.3$, $\Omega_\Lambda = 0.7$, and $H_0 = 70$ km s^{-1} Mpc^{-1}.

2. PG 1535+547

PG 1535+547 ($z = 0.038$, De Vaucouleurs et al. 1991) is a radio-quiet (ratio of radio-to-optical flux density[1] $R = 0.14$; Kellermann et al. 1989) type I AGN comprised in the Palomar-Green Bright Quasar Survey (PG BQS; Schmidt & Green 1983, $M_B = -20.8$ for the cosmology adopted in the present paper). Because of the narrow Hβ line ($FWHM(H\beta) = 1480$ km s^{-1}, Boroson & Green 1992; Véron-Cetty et al. 2001), the source is classified as Narrow Line Seyfert 1 (NLS1, which are historically defined to have $FWHM(H\beta) < 2000$ km s^{-1}, Osterbrock & Pogge 1987, and ratio of [O III]/H$\beta < 3$, Shuder & Osterbrock 1981). This AGN's optical spectrum presents strong Fe II emission lines (de Veny & Lynds 1969; Phillips 1978; Smith et al. 1997), as typically observed in NLS1 galaxies (Boroson & Green 1992; Sulentic et al. 2000; Grupe et al. 2004b). The optical/UV continuum appears substantially reddened (Smith et al. 1997) and polarized: its optical polarization, $P = 2.5\%$, is the highest among the PG sample (showing a $\langle P \rangle = 0.5\%$; Berriman et al. 1990). Strong intrinsic C IV λ1549 absorption features, blueshifted by ∼2500 km s^{-1} with respect to the redshift of the source (Sulentic et al. 2006) further classify the source as a "mini-broad absorption line (BAL) QSO"[2], and imply the presence of a moderate velocity outflow. Finally, no optical microvariability has been observed (Carini et al. 2007).

The mass of the central black hole of PG 1535+547 has been derived by Vestergaard & Peterson (2006) and Zhang & Wang (2006) using two slightly different versions of the relation with the optical continuum luminosity and the $FWHM(H\beta)$, and by Zhang & Wang (2006) by rescaling the stellar velocity dispersion estimated from the [O III] line. The three evaluations give $\log(M_{BH}/M_\odot) = 7.19$, 6.94, and 7.34, respectively. The slightly different M_{BH} derived from the $FWHM(H\beta)$ and using the [O III] line width suggests that the stellar velocity dispersion is larger than expected from the $FWHM(H\beta) - M_{BH}$ relation. For PG 1535+547, this would imply a location below the $M_{BH}-\sigma$ relation found for local galaxies (e.g., Tremaine et al. 2002). A similar result was found for other NLS1 galaxies accreting close to the Eddington limit (Grupe & Mathur 2004; Mathur & Grupe 2005), as in the case of PG 1535+547: the bolometric luminosity and the black hole mass estimated using the [O III] line from Zhang & Wang (2006) lead to an accretion rate relative to the Eddington rate of $\log \dot{m} = -0.32$. It is worth noting that both NLS1 and BAL QSO are found to lie at the extreme of the anti-correlation between [O III] and Fe II emission (the so-called Eigenvector 1; Boroson & Green 1992) observed in low-redshift QSO, which is thought to be driven by a high Eddington ratio (Boroson 2002).

In the X-ray band, *ROSAT* PSPC observations (1993) detected the source with a 0.1−0.4 keV count rate[3] of $(0.761 \pm 0.195) \times 10^{-2}$ cts s^{-1}. The source was not detected in the hard (0.5−2.0 keV) band, nor it is detected in the *ROSAT* All Sky Survey catalog[4]. Gallagher et al. (2001) estimated an upper limit to the observed count rate in the 0.5−2 keV energy range[5] of 3.2×10^{-3} cts s^{-1}. The nondetection above 0.5 keV reminds another NLS1, the X-ray transient WPVS 007. In their analysis of *ROSAT* data, Grupe et al. (1995) suggested obscuration as the possible cause of the turn-off observed in the 0.5−2.4 keV energy range. On the basis of the *ROSAT* observation, Brandt et al. (2000) classified PG 1535+547 as soft X-ray weak QSO.

[1] Measured at 6 cm and 4400 Å, respectively.

[2] Defined as QSO showing in their optical/UV spectrum absorption lines with intermediate widths between the "classical" BAL QSO (absorption line width ≥2000 km s^{-1}) and the narrow absorption line QSO (absorption line width ≤500 km s^{-1}); see e.g., Weymann et al. (1991); Narayanan et al. (2004).

[3] ftp://ftp.xray.mpe.mpg.de/rosat/catalogues/1rxp/

[4] http://www.xray.mpe.mpg.de/cgi-bin/rosat/src-browser

[5] The authors reported the detection of 5 photons above 0.5 keV in a 1′.2 radius source cell, with 2 expected from the background.

Table 1. EPIC XMM-Newton data observation log.

Obs. ID	Instrument	Filter	Date	Start End	Exp. [ks]	Net exp. time [ks]	Net count rates[a] [10^{-1} counts s^{-1}]	S/N[a]	Name used in the text
	MOS1	thin	2006 Jan. 24–25	22:16:06	25.7	20.64	9.5 ± 0.2	43.94	
				05:26:53			0.5 ± 0.1	10.20	
0300310501	MOS2	thick	2006 Jan. 24–25	22:16:06	25.7	21.60	8.6 ± 0.2	42.68	
				05:26:58			0.5 ± 0.1	9.87	
	pn	thin	2006 Jan. 24–25	22:38:48	24.0	15.61	34.1 ± 0.5	72.01	
				05:27:13			2.7 ± 0.1	20.04	*(A)*
	MOS1	thin	2006 Jan. 22–23	22:43:11	29.3	18.31	9.9 ± 0.2	42.11	
				06:53:58			0.5 ± 0.1	9.88	
0300310401	MOS2	thick	2006 Jan. 22–23	22:43:11	29.3	18.42	8.4 ± 0.2	39.04	
				06:54:03			0.5 ± 0.1	3.91	
	pn	thin	2006 Jan. 22–23	23:05:53	27.6	13.77	30.4 ± 0.5	63.82	
				06:54:18			2.7 ± 0.1	5.60	
	MOS1	thin	2006 Jan. 16–17	22:36:41	31.1	8.38	14.1 ± 0.4	30.15	
				07:17:28			0.4 ± 0.1	5.56	
0300310301	MOS2	thick	2006 Jan. 16–17	22:36:41	31.1	12.93	12.3 ± 0.3	39.54	*(B)*
				07:17:33			0.6 ± 0.1	8.84	
	pn	thin	2006 Jan. 16–17	22:59:23	29.4	5.80	46.7 ± 0.9	51.79	
				07:17:48			3.2 ± 0.2	13.48	
	MOS1	thin	2002 Nov. 03	01:06:17	29.5	24.53	4.0 ± 0.1	30.71	
				09:20:24			0.3 ± 0.1	7.98	
0150610301	MOS2	thin	2002 Nov. 03	01:06:17	29.5	24.53	4.1 ± 0.1	30.76	*Nov. 2002*
				09:20:24			0.3 ± 0.1	7.87	
	pn	thin	2002 Nov. 03	01:28:48	27.8	20.66	13.6 ± 0.3	49.58	
				09:20:44			1.8 ± 0.1	18.16	

[a] In the energy range 0.4–10 keV (*first line*) and 6.5–10 keV (*second line*).

In 1999, six years after the *ROSAT* observations, *ASCA* found that the source emission has varied in a significant way: assuming the best fitting *ASCA* spectral model, Gallagher et al. (2001) predicted a PSPC count rate of $4.9^{+1.1}_{-0.9} \times 10^{-3}$ cts s^{-1}, i.e. a factor ∼1.5 higher than the upper limit estimated for the *ROSAT* observation. Moreover, the authors found evidence of X-ray intrinsic absorption ($N_H \approx 10^{23}$ cm^{-2}) with only partial covering of the power-law continuum. The limited quality of the *ROSAT* data prevented the authors from ascribing the observed variation to an increase of the continuum flux or a decrease of the absorption. As noted by Gallo (2006), NLS1 galaxies with complex high-energy spectra (such as PG 1535+547) appear to be X-ray weak AGN.

The XMM-Newton observation performed in November 2002 found PG 1535+547 in a higher state than previous observations at energies $E > 2$ keV (Schartel et al. 2005). Moreover, the EPIC spectra clearly require the presence of a complex absorbing structure. A good description of the data is obtained only assuming a combination of an ionized absorber and a neutral absorber with a large covering factor. Finally, the data suggest the presence of a broad emission feature, whose profile is well described by a relativistically broadened Fe Kα emitted in a disk accreting around a black hole. The absence of a feature like this in the *ASCA* data allowed the authors to suggest a possible variability in the emission line. A similar behavior (i.e., complex X-ray emission and strong variability) has been reported for other NLS1s: for example, Grupe et al. (2007) found Mrk 335 in an extremely low X-ray state, whose interpretation includes partial-covering absorption or X-ray reflection from the disk. A comparison of the emission observed in 2007 with all previous observations shows a decrease in flux by a factor of more than 30, which the authors ascribe mainly to a change of the intrinsic absorption.

3. Observation and data reduction

We observed PG 1535+547 (RA = 15:36:38.3, Dec = +54:33:33) with XMM-Newton in January 2006 in three pointings, the first separated by about one week from the others, for a total of about 90 ks (Obs. ID 0300310301, 0300310401 and 0300310501). We performed the observations with the European Photon Imaging Camera (EPIC), the Optical Monitor (OM) and the Reflection Grating Spectrometer (RGS; den Herder et al. 2001); we did not detect the source with the RGS. The three EPIC cameras (pn, MOS1, and MOS2; Strüder et al. 2001; Turner et al. 2001) were operating in full frame mode, MOS1 and pn with the thin filter and MOS2 with the thick filter applied. The observation details are reported in Table 1. OM (Mason et al. 2001) performed 6 observations for each pointing, three with the *UVM2* (λ_{eff} = 2310 Å) and three with the *UVW2* (λ_{eff} = 2120 Å) filters in the optical light path, of 1.9 ks each; all OM exposures were performed in the "science user defined" image mode (with a windows size of 5′ × 5′). We processed the XMM-Newton data with the Science Analysis Software (SAS version 7.0) with the calibration from February 2007; we ran the tasks *epproc* and *emproc* to produce calibrated and concatenated event lists for the EPIC cameras.

EPIC event files have been filtered for high-background time intervals, following the standard method consisting in rejecting periods of high count rate at energies >10 keV. We used events corresponding to patterns 0–12 (MOS1&2) and 0–4 (pn; see the XMM-Newton Users' Handbook; Ehle et al. 2001). We also generated the spectral response matrices at the source position with the SAS tasks *arfgen* and *rmfgen*. We can exclude event pile-up in the MOS and pn data. Source counts were extracted from a circular region of radius 18″ and 21″ for the MOS and pn. Background counts were extracted from a nearby source-free circular region of 36″ and 42″ radii, respectively. The net exposure times at the source position, the net count rates and the S/N ratios in the energy ranges 0.4–10 keV and 6.5–10 keV are reported in Table 1.

We tested short time variability within each observation, generating source light curves in different energy ranges with a binning time of 5 ks. No bin shows significant deviation from the mean value.

Table 2. OM integrated magnitudes and fluxes (January 2006 observations).

Obs. ID	AB magnitudes [mag]		Flux [10^{-15} ergs cm^{-2} s^{-1} Å^{-1}]	
	UVM2 [2310 Å]	*UVW2* [2120 Å]	*UVM2* [2310 Å]	*UVW2* [2120 Å]
0300310501	16.567 ± 0.016	16.719 ± 0.027	4.811 ± 0.069	4.977 ± 0.123
0300310401	16.510 ± 0.015	16.648 ± 0.026	5.072 ± 0.071	5.312 ± 0.127
0300310301	16.496 ± 0.015	16.625 ± 0.025	5.139 ± 0.071	5.427 ± 0.127

We processed OM data with the *omichain* routine of SAS; we obtained three images for each OM filter and for each pointing. The count rate informations were extracted from the three *omichain* output and averaged, assuming the standard deviation as an estimate of their error. The count rates were converted to magnitudes (in the AB system) and fluxes using the conversion factors reported by the SAS homepage[6]; the errors were calculated propagating the uncertainties on the count rates. We provide the obtained values in Table 2; in all the observations, the ratio of the maximum to the minimum count rates is consistent with unity within the errors.

In order to better compare the old and new XMM-Newton observations, we have re-analyzed the EPIC XMM-Newton data taken in November 2002 (archived under the observation identifier 0150610301). At this occasion, PG 1535+547 was not observed with OM. Following Schartel et al. (2005), we determined for the two MOS exposures the background from an annulus around the extraction area of the source counts (inner and outer radii: 48″ and 84″, respectively). Details of this observation, as well as exposure times, count rates and S/N ratios in the energy ranges 0.4−10 keV and 6.5−10 keV, are reported in Table 1.

4. The X-ray emission: a first comparison between the datasets

We performed the spectral analysis of the MOS and pn spectra over the energy range from 0.4 keV to 10.0 keV. We analized the EPIC spectra with standard software packages (FTOOLS version 6.2, XSPEC version 12.3.1q, XSPEC version 11.3.2ag; Arnaud 1996). All the models discussed in the following assume Galactic absorption with a column density of $N_{\rm H,\,Gal} = 1.35 \times 10^{20}$ cm^{-2} (Murphy et al. 1996). Unless otherwise stated, the figures are in the rest-frame of PG 1535+547, and fit parameters are quoted in the same frame.

Comparing the three observations of January 2006, it is evident that the flux decreases considerably passing from the observation 0300310301 to the other two, which present the same spectral shape and intensity. This behavior is particularly enhanced at energies lower than 0.7 keV. Therefore, we combined the pn and MOS data from 0300310401 and 0300310501 (the label A identifies the combined spectra), keeping the 0300310301 data, which are labeled as B, separate. In order to apply the χ^2 statistics, source counts for the (A) and (B) spectra were binned to have at least 40 and 30 counts in each energy bin, respectively.

From a comparison between the new and the old datasets, a strong change of both flux and spectral shape is evident (see Fig. 1, *left panel*).

In Fig. 1, *right panel*, we plotted the ratio of the January 2006 XMM-Newton spectra of PG 1535+547 to the November 2002 data (considering that the MOS spectra agree, within the errors, with the EPIC-pn spectra, to avoid clutter, only the last are shown). The best fit found by Schartel et al. (2005) for the November 2002 data–an intrinsic power law with a superimposed, relativistically-broadened line emitted by an accretion disk around a Kerr black hole, covered by a combination of an ionized absorber and a neutral absorber with a large covering factor-cannot describe either the (A) data or the (B) spectra. This figure may offer a first indication of the origin of the observed emission. The strongest variation is observed in the soft energy band, with the emission between 0.7 and 1.5 keV being less affected by changes. This ratio would imply that the observed variability is associated mainly with absorbing matter whose physical properties (i.e., location, column density, and/or ionization state) are different among the observations.

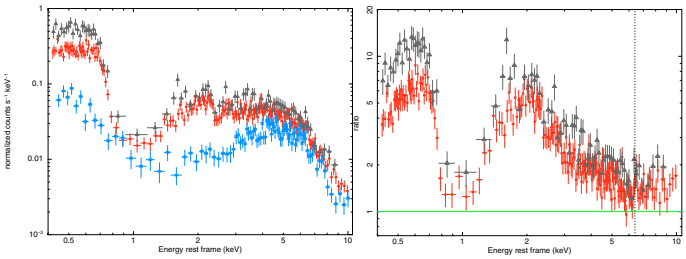

Fig. 1. *Left panel*: EPIC-pn spectra of the three observations: red-filled circles, spectrum (A); grey-open triangles, spectrum (B); sky-blue stars, November 2002 data. *Right panel*: ratios between the new EPIC-pn spectra and the best fit model for the November 2002 dataset (Schartel et al. 2005). The black-dotted line corresponds to the position of the 6.4 keV line.

5. Spectral analysis of the January 2006 (A) data

We started with the (A) data, due to the higher S/N of these spectra. We performed the analysis of the November 2002 and the (B) datasets taking into account the results of the first part of the work.

5.1. The emission at energies >3.5 keV

First, we fitted the (A) data with a simple power law. Due to the complex spectral shape both at low and high energies, we considered only the 3.5−5 keV energy range, finding a photon index $\Gamma = 1.40 \pm 0.19$. This spectral index appears flatter than the mean value found at energies >2 keV for a sample of AGN selected in the PG BQS ($\langle\Gamma\rangle = 1.87 \pm 0.10$; Piconcelli et al. 2005). This discrepancy is even stronger considering only NLS1 galaxies, whose photon indices appear to be on average steeper than those of Seyfert galaxies with broad optical lines (e.g., studying *ASCA* spectra of 23 NLS1s, Leighly 1999 found a mean value in the 2−10 keV energy range $\langle\Gamma\rangle = 2.19 \pm 0.10$). When the model is extrapolated to the whole 0.4−10 keV band, the most evident feature is a strong decrease in the flux below 3 keV, particularly enhanced between 0.7 and 2 keV (Fig. 2, *upper panel*).

Focusing at $E > 3.5$ keV, this simple model shows residual structures in the 5.5−6.5 keV rest frame region, and is also unable to describe the high-energy end of the spectra (Fig. 2, *lower panel*).

To model the observed residuals, as a first step, we added one or more narrow or broad line(s) to the power-law continuum (ZGAUSS component in XSPEC, with $\sigma = 1$ eV or free to vary), and/or an absorption edge at ∼7 keV (ZEDGE component

[6] http://xmm.vilspa.esa.es/sas/7.0.0/watchout/Evergreen_tips_and_tricks/uvflux.shtml

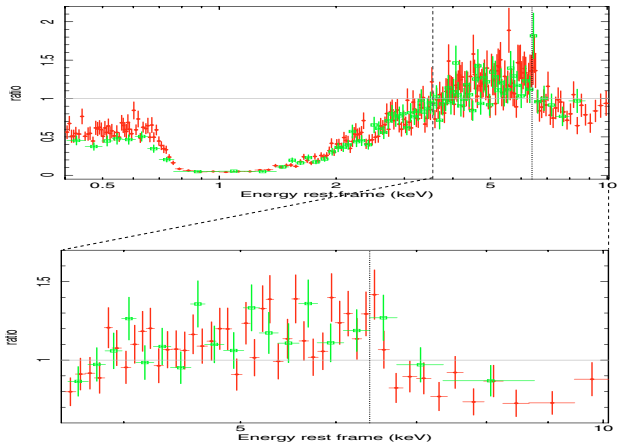

Fig. 2. Data/model ratio for the (A) spectra (green open squares, MOS; red filled circles, pn). The adopted model is a simple power law with Galactic absorption fitted between 3.5 and 5 keV, and extrapolated up to 10 keV (*lower panel*), and to the whole studied energy range (0.4−10 keV, *upper panel*; for demonstration purposes, here the data have been binned to have a significance of 8σ up to 30 bins). In both panels, the black-dotted line marks the position of the 6.4 keV line.

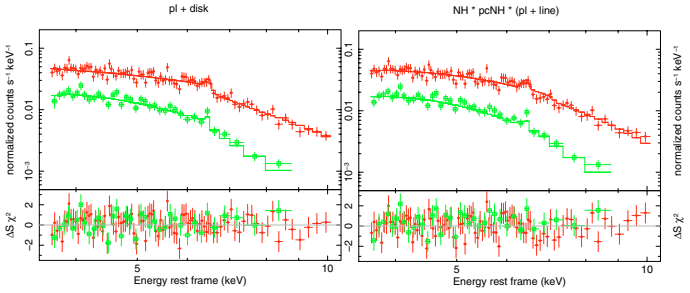

Fig. 3. EPIC-pn January 2006 (A) spectra of PG 1535+547 in the 3.5−10 keV energy range, plotted in comparison to the reflection-based (*left panel*) and the absorption-based (*right panel*) models (see Sect. 5.1 and Table 3).

in XSPEC). The addition of the absorption edge cannot reproduce the data between 6 and 7 keV, and still required an unusually low photon index, $\Gamma \sim 1.27$. The observed spectra can be well described assuming a model with two Gaussian lines, one narrow and one broad, whose energies were consistent with being produced by neutral iron, or a power-law model with a superimposed disk line in a Kerr configuration (LAOR component in XSPEC; Laor 1991; Fabian et al. 2002). The addition of a narrow Gaussian line with energy consistent with being produced by matter in low-ionization stages (i.e., Fe I-Fe XVII) improves the fit significantly (F-test probability[7] 97.3%). Being the line unresolved by EPIC-pn, in the following its width has been fixed to the instrumental spectral resolution.

In the last years, two different scenarios have been proposed to account for high-energy spectral shapes as observed in the (A) spectra (Fig. 2, *lower panel*): a "reflection-based" (e.g., Mrk 335, Longinotti et al. 2007; O'Neill et al. 2007; HE 0450-2958, Zhou et al. 2007) or an "absorption-based" (e.g., 1H 0707-495, Boller et al. 2002; Gallo et al. 2004; Fabian et al. 2004; Tanaka et al. 2004; 1H 0419-577, Pounds et al. 2004; Fabian et al. 2005; IRAS 13197-1627, Dadina & Cappi 2004; Miniutti et al. 2007) one. Despite their different shape in the Fe-line energy region, the superposition of different layers of partially-ionised absorbing material could mimic the presence of a broad line component superimposed to the continuum, a feature naturally present in a relativistically-blurred, ionized reflection model (see e.g. Reeves et al. 2004; Grupe et al. 2007; Petrucci et al. 2007).

A reflection component can easily reproduce the high-energy curvature (with χ^2/d.o.f. = 109.2/119) only if it originates in the accretion disk[8], leading to a rather steep intrinsic continuum, $\Gamma \sim 2.3$. To model the ionized reflection in XSPEC, we used the REFLION[9] external table, which incorporates both line emission with Compton broadening and reflection continuum (Ross & Fabian 2005; Ross et al. 1999). Then, the reflection from the disk has been modeled by convolving this component with the relativistic blurring model KDBLUR, produced by Fabian and Johnstone using the same kernel of the LAOR disk line model[10].

The 3.5−10 keV data can be equally well reproduced (χ^2/d.o.f. = 121.3/123) in an absorption scenario, assuming a high column density ($N_{\rm H} \sim 10^{23}$ cm^{-2}) cold absorber covering ~80% of the primary continuum. This latter component is rather steep ($\Gamma \sim 2.5$), to account for the observed spectral drop at the highest energies ($E > 7$ keV). Allowing the ionization state of the absorbers or the iron abundance to be free parameters, the fit does not improve further.

The high-energy curvature observed in the (A) spectra of PG 1535+547 can thus be well accounted for in both reflection-based and absorption-based scenarios (see Table 3 and Fig. 3). A gaussian emission line is detected with an F-test probability of 98.6% in both cases; its energy and EW (~50−80 eV) are compatible with Kα fluorescence emission of almost neutral iron, produced by transmission through cold gas of column density $<10^{23}$ cm^{-2} totally covering the source (Makishima 1986).

5.2. The whole energy range

We then extended the analysis at all energies (0.4−10 keV). The (A) spectra between ~0.7 and 2 keV appear strongly absorbed, with an important component rising in the softer band. Evident absorption features are present at $E \sim 2$ keV as well as at energies lower than about 0.7 keV. Simple models, composed by a single-power law continuum covered by a combination of neutral or ionized absorbers (modeled with ABSORI component in XSPEC; Zdziarski et al. 1995), were not able to reproduce the observed shape. A model based only on reflection from neutral material distant from the black hole was not able to explain the observed emission, either. More complex scenarios have to be investigated.

The basic models adopted to test the reflection-based and the absorption-based scenarios are described in Sect. 5.1:

- a power law plus reflection from the disk (the latter constructed in XSPEC using the REFLION external table convolved with the KDBLUR model);
- a simple power law and a complex partial covering material.

[7] But see the caveats in using the F-test to measure the significance of narrow lines described in Protassov et al. (2002).

[8] Reflection from neutral material far from the nucleus (PEXRAV in XSPEC; Magdziarz & Zdziarski 1995) does not provide a good description of the data (χ^2/d.o.f. = 132.2/121).

[9] http://heasarc.gsfc.nasa.gov/docs/xanadu/xspec/models/reflion.html

[10] Unless otherwise stated, the outer radius was fixed to its maximum value, $R_{\rm out} = 400\ r_{\rm g}$, while the inner radius and the emissivity power-law index were free to vary.

Table 3. Analysis of the high energy (3.5−10 keV) part of the January 2006 (A) pn and MOS spectra.

Results for a reflection-based model.

Model	Power Law + Gaussian†			Kdblur[Reflion]‡			χ^2/d.o.f.
	Γ	Norm[a]	E_{rf} [keV]	β	R_{in} [GM/c^2]	i [°]	
				Fe/solar	ξ[b]	Norm[c]	
DISK+LINE	$2.32^{+0.96}_{-0.13}$	$6.40^{+1.89}_{-1.28}$	6.46 ± 0.04	$3.02^{+0.27}_{-0.39}$	$3.85^{+1.16}_{-2.39}$	$0.02^{+0.05}_{-0.01}$	109.2/119
				$1.25^{+4.99}_{-0.22}$	$159.59^{+177.14}_{-127.41}$	$4.26^{+0.24}_{-0.17}$	

Results for an absorption-based model.

Model	Power Law + Gaussian†			PC Absorber		Absorber	
	Γ	Norm[a]	E_{rf} [keV]	N_H[d]	Cov. fraction[e]	N_H[d]	χ^2/d.o.f.
NEUTRAL PC+LINE	$2.55^{+0.25}_{-0.20}$	$40.87^{+10.82}_{-13.34}$	$6.41^{+0.07}_{-0.05}$	$10.79^{+1.62}_{-2.22}$	$0.80^{+0.20}_{-0.09}$	$3.24^{+1.08}_{-1.11}$	121.3/123

Errors are quoted at the 90% confidence level for 1 parameter of interest ($\Delta\chi^2 = 2.71$). † Narrow line width fixed to 0 eV. ‡ Photon index coupled with the primary power-law photon index; outer radius fixed to the maximum value, $R_{out} = 400\,r_g$. [a] In units of 10^{-4} photons keV^{-1} cm^{-2} s^{-1} @1 keV. [b] Ionization parameter $\xi \equiv 4\pi F_{ill}/n$ (erg cm s^{-1}), where F_{ill} is the ionizing flux and n is the hydrogen nucleus density (part cm^{-3}) of the illuminated slab. [c] In units of 10^{-6} photons keV^{-1} cm^{-2} s^{-1} @1 keV of the reflected spectrum. [d] In units of 10^{22} cm^{-2}. [e] Complement to one of the covered-to-uncovered flux ratio.

Table 4. Analysis of the broadband January 2006 pn and MOS spectra (0.4−10 keV).

Result for a warm absorber∗[partial covering warm absorber∗(intrinsic power law+disk reflection)+narrow line] model.

Obs.	Power Law		PC Warm Absorber			Warm Absorber		Kdblur[Reflion]†			χ^2/d.o.f.
	Γ	Norm[a]	N_H[b]	ξ[c]	Cov. fraction[d]	N_H[b]	ξ[c]	β	R_{in} [r_g]	ξ[c]	
								i [°]	Fe/solar	Refl. fraction[e]	
(A)	2.06±0.08	$3.21^{+1.81}_{-1.03}$	$6.11^{+2.04}_{-1.36}$	$68.14^{+34.15}_{-20.77}$	$0.78^{+0.08}_{-0.12}$	2.13±0.08	3.67±0.08	$4.34^{+0.34}_{-0.27}$	$1.31^{+1.39}_{-0.07}$	$121.59^{+40.48}_{-52.22}$	290.1/281
								0.003 ± 0.01	$4.54^{+0.35}_{-1.01}$	65.2%	

Result for a neutral absorber∗{warm absorber∗[partial covering warm absorber∗(intrinsic power law)]+scattered component+narrow lines} model.

Obs.	Power Law‡		PC Warm Abs.			Warm Abs.		Gaussian		Neutral Abs.	χ^2/d.o.f.
	Γ	Norm[a]	N_H[b]	ξ[c]	Cov. fraction[d]	N_H[b]	ξ[c]	E_{rf}[f]	σ[g]	N_H[b]	
	Γ_{scatt}	Scatt. fraction[h]									
(A)	$2.43^{+0.13}_{-0.03}$	$22.74^{+10.19}_{-8.06}$	$8.43^{+1.26}_{-1.54}$	$19.96^{+4.53}_{-3.15}$	$0.43^{+0.03}_{-0.11}$	$4.49^{+0.17}_{-0.12}$	$94.04^{+0.98}_{-1.73}$	$0.59^{+0.01}_{-0.02}$	< 30	$0.21^{+0.02}_{-0.02}$	297.5/279
	$2.83^{+0.39}_{-0.67}$	$0.006^{+0.002}_{-0.001}$									

Errors are quoted at the 90% confidence level for 1 parameter of interest ($\Delta\chi^2 = 2.71$); narrow-line energy fixed to $E_{rf} = 6.4$ keV, narrow-line width fixed to 0 eV. † Photon index coupled with the primary power-law photon index; outer radius fixed to the maximum value, $R_{out} = 400\,r_g$. ‡ First line, intrinsic power law; second line, scattered power law. [a] In units of 10^{-4} photons keV^{-1} cm^{-2} s^{-1} @1 keV. [b] In units of 10^{22} cm^{-2}. [c] Ionization parameter $\xi \equiv 4\pi F_{ill}/n$ (erg cm s^{-1}), where F_{ill} is the ionizing flux and n is the hydrogen nucleus density (part cm^{-3}) of the illuminated slab. [d] Complement to one of the covered-to-uncovered flux ratio. [e] Ratio between the ionized-reflection flux and the total flux in the (0.1−1000) keV energy range. [f] Line centroid energy, in keV. [g] Line width, in eV. [h] Ratio between the scattered flux and the primary, unabsorbed flux.

The overall broadband shape was roughly reproduced by the two models, although in the latter case the strong soft excess observed can be partially accounted for only allowing the absorbing column densities to be ionized. Under this assumption, the absorbers are able to transmit the nuclear flux at low energies. However, these simple models were inadequate to model the absorption features, resulting in statistically unacceptable fits.

For the reflection-based model, following the best fit obtained in Sect. 5.1, we adopted a continuum model composed by an intrisic power law and a relativistically blurred ionized reflection. To model the absorption features observed in the spectra, we assumed the presence of a warm absorber partially covering the central region along with a second distribution of matter with lower ionization covering the whole emission. Finally, a transmitted narrow line at 6.4 keV (rest frame) completes the model. This complex model resulted in a good description of the (A) data (χ^2/d.o.f. = 290.1/281); the best fit parameters are shown in the first part of Table 4.

As previously noted, the presence of ionized absorption can affect the high-energy spectrum and the iron line profile. We then checked our results modeling the absorber in a more sophisticated way, adopting a more refined photoionization model, namely XSTAR[11] (Kallman & Bautista 2001). XSTAR is a public code that consistently (i.e., by solving temperature and ionization balance equations) calculates the opacities of a spherical shell of Compton-thin gas photoionized by a central source of radiation. It offers the possibility of constructing tables varying the photoionizing continuum spectral shape and strength, the gas physical conditions (density, pressure, thickness), and the abundances of cosmic elements. Its atomic database includes all the most relevant transitions. To perform the fit using

[11] http://heasarc.gsfc.nasa.gov/docs/software/xstar/xstar.html

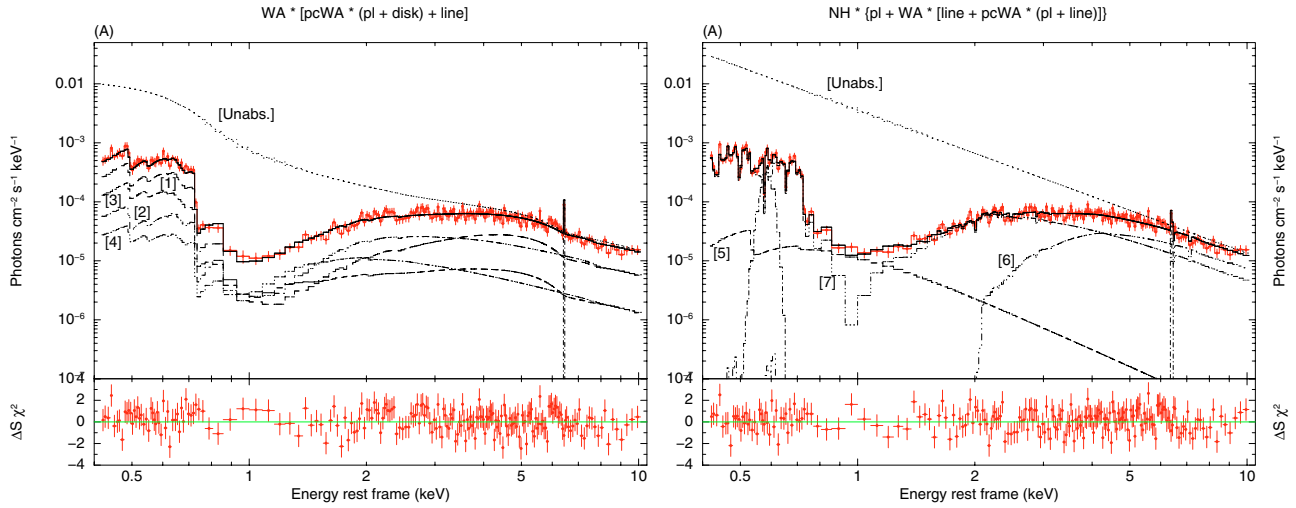

Fig. 4. Comparison of the unfolded best fits to the EPIC-pn January 2006 (A) data of PG 1535+547 with the two adopted models (see Sect. 5.2; *upper panels*). The residuals in terms of sigmas are plotted in the *lower panels*. The solid lines correspond to the total best fit models; over-plotted are the contributions of the different components. The unabsorbed emission, labeled as [Unabs.], is also shown. *Left panels*: reflection from the disk (dashed line) and intrinsic power law (dash-dot-dotted line) partially covered by an warm absorber (the thickest lines identify the fraction of continuum covered, [1] and [2] respectively; the thinnest lines identify the fraction uncovered, [3] and [4] respectively), with a narrow line superimposed (dash-dotted line); the whole continuum was seen through a secon ionized layer of material. *Right panels*: scattered component (dashed line, [5]), absorbed power law (dash-dot-dotted line) and narrow-emission lines (dash-dotted line), partially covered by an warm absorber (the thickest line identify the fraction of continuum covered, [6], the thinnest the fraction uncovered, [7]); the whole continuum was seen through layer of neutral material.

XSPEC version 12[12], we considered $N_{\rm H}$ to be a free parameter but keeping its value fixed during the minimization. The best fitting parameters are in good agreement with the values reported in the first part of Table 4, while the fit obtained with this change in the absorption model is statistically worse. Above all, a disk component is still statistically required.

Regarding the two-phase warm absorber-based scenario, to improve the fit ($\Delta\chi^2/\Delta$d.o.f. = 14.9/1), we added a soft power law component absorbed only by neutral gas to the power law (covered by an ionized, partial covering absorber and an ionized, fully covering absorber). If we allow the soft power-law photon index to be a free parameter, the fit improves significantly but still remains statistically poor (χ^2/d.o.f. = 350.0/279). Looking at the residuals, it seems that the ABSORI model is inadequate to describe the complex shape of the absorbing structure seen at 0.7−1 keV. Moved by these considerations, we try to reproduce the soft complexities with the cited XSTAR tables.

In order to apply these tables, for this part of the analysis, we turned to XSPEC version 11. We fitted to the data our model (a double-ionized absorber, one partially covering and the other totally covering the source, plus a soft-scattered component), using a pre-calculated XSTAR table. The publicly available table "grid 18b" assumes a 10^{44} erg s^{-1}, Γ = 2 power law ionizing a constant density shell of gas whose abundances can be varied. The turbulent velocity of gas is assumed to be 100 km s^{-1}. We obtained a good fit to the data with an oxygen overabundance of ∼4 × solar, requested to reproduce the deep absorption structure observed between 0.7 and 1 keV. We note here that an ionizing continuum steeper than Γ = 2 results in deeper resonant absorption in this energy range due to the higher number of soft-ionizing photons (see e.g., Nicastro et al. 1999). If a grid generated assuming a continuum with Γ = 2.5 is applied to the model, no oxygen overabundance is needed to reproduce the depth of the absorption structure; however, in this case the enhanced opacities at low energies (E < 0.7 keV) cannot reproduce the flat spectra observed in this energy range. We decided to proceed with the analysis adopting the "grid 18b" table with these considerations in mind.

A visual inspection of data/model ratio shows an excess of emission in the soft band. The addition of a Gaussian emission line improves the fit. The line energy, E ∼ 0.59 keV, is fully compatible with the photoionized O VII triplet energy. Soft X-ray emission lines, mainly O VII or Ne IX, have been found in the spectrum of other Seyfert galaxies (e.g., Mrk 6, Immler et al. 2003; Mrk 1239, Grupe et al. 2004a; Mrk 304, Piconcelli et al. 2004; Guainazzi & Bianchi 2007 and references therein). Broad components of the O VII triplets associated with the BLR have been observed in the X-ray spectra of the bright NLS1 Mrk 110 (Boller et al. 2007) and of the Seyfert galaxy Mrk 279 (Costantini et al. 2007). Unfortunately, the flux of PG 1535+547 is too low and prevents us from drawing information from the RGS spectra.

The best fit model results in a moderately-ionized gas ($N_{\rm H}$ ∼ 8.4 × 10^{22} cm^{-2}, ξ ∼ 19.9 erg cm s^{-1}) covering ∼40% of the primary emission, a second absorber with lower column density and higher ionization state ($N_{\rm H}$ ∼ 4.5 × 10^{22} cm^{-2}, ξ ∼ 94 erg cm s^{-1}) fully covering the source, a scattered component and two gaussian emission lines (Fe and O VII). The absorbed power law is rather steep (Γ ∼ 2.5) and the scattered one is even steeper, as expected if scattering occurs in a photoionized gas. Finally, the whole emission is covered by a neutral absorber with a rather low column density ($N_{\rm H}$ ∼ 2 × 10^{21} cm^{-2}). This complex model results in an equally good description of the (A) spectra (χ^2/d.o.f. = 297.5/279, see second part of Table 4). For

[12] The model assumed to describe the reflection from the disk taking into account the relativistic blurring can be fitted only inside the new version of XSPEC. On the other hand, using the XSTAR tables in the last version of XSPEC, the minimization algorithm encounters problems in interpolating the column density values between grid points. Their origin is currently under investigation (Craig Gordon, priv. comm.).

Table 5. Simultaneous analysis of the three available XMM-Newton datasets for PG 1535+547 in the 0.4−10 keV energy range. The adopted model was the accretion disk reflection model: a continuum composed by an intrinsic power law and a reflection from the disk partially covered by an ionized absorber; the whole continuum was seen through a warm absorber (χ^2/d.o.f. = 379.6/364).

	Power Law		PC Warm Absorber			Warm Absorber		Kdblur[Reflion]†		
Obs.	Γ	Norm^a	$N_H{}^b$	ξ^c	Cov. fraction^d	$N_H{}^b$	ξ^c	β	R_{in} [r_g]	ξ^c
								i [°]	Fe/solar	Refl. fraction^e
(A)	$2.05^{+0.05}_{-0.12}$	$2.76^{+0.98}_{-0.77}$	$5.77^{+1.97}_{-1.90}$	$55.19^{+25.86}_{-24.74}$	0.72 ± 0.08	$2.07^{+0.18}_{-0.28}$	$3.28^{+0.70}_{-1.46}$	$4.26^{+0.23}_{-0.27}$	$1.31^{+1.20}_{-0.07}$	$130.71^{+10.11}_{-19.31}$
								$(2.7 \pm 0.6) \times 10^{-3}$	$4.71^{+0.87}_{-1.83}$	48.8%
(B)	$2.05^\ddagger$	$2.57^{+0.55}_{-1.01}$	$3.44^{+2.13}_{-1.28}$	$66.62^{+39.88}_{-32.57}$	0.85 ± 0.06	$2.07^\ddagger$	$3.28^\ddagger$	$4.26^\ddagger$	$1.31^\ddagger$	$125.97^{+12.14}_{-9.65}$
								$(2.7 \times 10^{-3})^\ddagger$	$4.71^\ddagger$	60.1%
Nov. 2002	$1.79^{+0.10}_{-0.09}$	$1.55^{+0.35}_{-0.96}$	$20.94^{+4.46}_{-2.87}$	$98.87^{+30.08}_{-25.81}$	$0.92^{+0.03}_{-0.01}$	$0.54^{+0.25}_{-0.36}$	$3.28^\ddagger$	$4.26^\ddagger$	$1.31^\ddagger$	$65.43^{+21.50}_{-17.23}$
								$(2.7 \times 10^{-3})^\ddagger$	$4.71^\ddagger$	45.0%

	Observed flux [10^{-13} ergs cm^{-2} s^{-1}]				Unabsorbed luminosity [10^{43} erg s^{-1}]			
Obs.	0.4−10 keV	0.4−1 keV	1−3 keV	3−10 keV	0.4−10 keV	0.4−1 keV	1−3 keV	3−10 keV
(A)	$25.54^{+13.30}_{-10.63}$	$1.52^{+1.24}_{-0.93}$	$3.11^{+1.64}_{-1.21}$	$20.90^{+10.42}_{-8.49}$	2.07	0.88	0.39	0.80
(B)	$33.53^{+28.25}_{-18.30}$	$2.74^{+2.30}_{-1.58}$	$4.16^{+4.12}_{-2.42}$	$26.63^{+21.83}_{-14.31}$	2.61	1.18	0.44	1.00
Nov. 2002	$15.14^{+10.74}_{-5.60}$	$0.37^{+0.69}_{-0.17}$	$0.94^{+0.37}_{-0.56}$	$13.84^{+5.04}_{-9.08}$	0.96	0.14	0.19	0.63

Errors are quoted at the 90% confidence level for 1 parameter of interest ($\Delta\chi^2 = 2.71$). Luminosity are absorption-corrected, while fluxes are corrected only for the Galactic absorption. Narrow-line energy fixed to $E_{rf} = 6.4$ keV. For the accretion disk reflection component, the outer radius was fixed to the maximum value, $R_{out} = 400\, r_g$. † For the single state, the power law and the accretion disk reflection components have the same photon index. ‡ Parameters for the states tied in the fit. ^{a} In units of 10^{-4} photons keV^{-1} cm^{-2} s^{-1} @1 keV. ^{b} In units of 10^{22} cm^{-2}. ^{c} Ionization parameter $\xi \equiv 4\pi F_{ill}/n$ (erg cm s^{-1}), where F_{ill} is the ionizing flux and n is the hydrogen nucleus density (part cm^{-3}) of the illuminated slab. ^{d} Complement to one of the covered-to-uncovered flux ratio. ^{e} Ratio between the ionized-reflection flux and the total flux in the (0.1−1000) keV energy range.

comparison, in Fig. 4 we have plotted the unfolded best fits to the pn data obtained with a partially-absorbed accretion disk reflection (*left panel*), or a combination of ionized absorbing layers and the addition of scattered emission (*right panel*).

We cannot test a partially-ionized absorbing material with large velocity shear (the SWIND[13] model in XSPEC, originally proposed by Gierliński & Done 2004 and updated by Gierliński & Done 2006) as the origin of the observed soft excess because the maximum column density assumed in the analytical model ($N_H \sim 8 \times 10^{22}$ cm^{-2}) is lower than the value we need to reproduce the high-energy spectral shape.

6. The origin of X-ray variability: comparison among the different XMM-Newton datasets

The physical scenarios explored in previous section to describe the (A) data yielded two complex models, composed by several continuum components and different absorbers. Both models are statistically acceptable. We then explored the possibility of explaining the variability observed between November 2002 and January 2006 (both in shape and intensity) by changing only the best fit parameters (but assuming the same components in the model): we applied the models described in Sect. 5.2 to the November 2002 and (B) datasets. The two models provide a good description for the two spectra with reasonable values for the model parameters. In the absorption-based model, the soft gaussian emission line at ∼0.57 keV is not requested by the November 2002 dataset: its *EW* upper limit is 273 eV at 90% confidence level. To conclude the analysis, we tested the possibility of fitting these models to the three states simultaneously, changing as few parameters as possible.

The large number of variables involved in the reflection-based model (some of them degenerate in the fit) can make it difficult to identify the parameters responsible for the observed variations. To choose the free parameters, we started by fitting the spectra simultaneously with all but the normalization tied toghether. We then thawed one parameter at a time, searching for an improvement in the fit. We repeated the same step with an increasing number of free parameters, in various combinations, until the improvement is no longer significant (i.e., F-test probability lower than 95%). In the final fit, the parameters identified in this way were kept free, while the parameters that seems don't vary were tied between the states. Variations in the inner-ionized absorber, partially covering the central source, coupled with an increase of the reflection fraction, produce the differences observed between (A) and (B) spectra. To explain the change between November 2002 and January 2006, both absorbing layers must vary; a lower accretion disk ionization state in the oldest observation is also required.

The absorption-based model can reproduce the three spectra by varying three parameters: the intrinsic power-law normalization, the covering fraction of the inner absorber and the ionization parameter of the outer absorber. The power-law normalization varies roughly proportional to the observed hard (3−10 keV) flux. Variations observed between (A) and (B) datasets can be explained by means of a different covering fraction of the inner-ionized absorber. The differences between November 2002 and January 2006 spectra can be attributed to a different covering fraction of the inner absorber plus a variation of the ionization state of the outer absorber.

The adopted models are able to describe the three states in a consistent way (χ^2/d.o.f. = 379.6/364 and 417.5/376; see Fig. 5): the best fit value for the parameters are reported in Tables 5 and 6.

[13] http://heasarc.gsfc.nasa.gov/docs/xanadu/xspec/models/swind1.html

Table 6. Simultaneous analysis of the three available XMM-Newton datasets for PG 1535+547 in the 0.4−10 keV energy range. The adopted model was the complex absorption scenario: an ionized, partially covering absorber plus a scattered component emerging from an ionized layer that fully covers the source (χ^2/d.o.f. = 417.5/376).

	Power Law†		PC Warm Abs.			Warm Abs.		Gaussian		Neutral Abs.
Obs.	Γ	Norm[a]	N_H[b]	ξ[c]	Cov. fraction[d]	N_H[b]	ξ[c]	E_{rf}[e]	σ[f]	N_H[b]
	Γ_{scatt}	Scatt. fraction[g]								
(A)	$2.54^{+0.63}_{-0.49}$	$32.56^{+12.00}_{-5.17}$	$8.24^{+5.53}_{-1.12}$	$18.16^{+7.23}_{-2.18}$	0.62 ± 0.03	$3.95^{+0.42}_{-0.23}$	$91.32^{+2.81}_{-2.03}$	0.56 ± 0.02	40 ± 30	$0.22^{+0.05}_{-0.01}$
	$2.90^{+0.65}_{-0.47}$	$0.005^{+0.004}_{-0.002}$								
(B)	2.54‡	$37.33^{+6.56}_{-7.77}$	8.24‡	18.16‡	$0.51^{+0.04}_{-0.03}$	3.95‡	91.32‡	0.56‡	40‡	0.22‡
	2.90‡	0.004 ± 0.001								
Nov. 2002	2.54‡	$30.60^{+13.43}_{-4.34}$	8.24‡	18.16‡	$0.91^{+0.03}_{-0.04}$	3.95‡	$60.69^{+10.10}_{-23.56}$	0.56‡	40‡	0.22‡
	2.90‡	$0.007^{+0.002}_{-0.003}$								

	Observed flux [10^{-13} ergs cm^{-2} s^{-1}]				Unabsorbed luminosity [10^{43} erg s^{-1}]			
Obs.	0.4−10 keV	0.4−1 keV	1−3 keV	3−10 keV	0.4−10 keV	0.4−1 keV	1−3 keV	3−10 keV
(A)	$25.30^{+5.55}_{-0.59}$	1.53 ± 0.01	$3.18^{+0.18}_{-0.02}$	$20.59^{+5.38}_{-0.57}$	5.70	2.72	1.87	1.11
(B)	$33.15^{+2.48}_{-1.48}$	2.60 ± 0.01	$4.48^{+0.09}_{-0.03}$	$26.06^{+2.41}_{-1.43}$	7.24	3.55	2.31	1.38
Nov. 2002	$14.93^{+1.54}_{-2.12}$	$0.35^{+0.01}_{-0.02}$	$0.94^{+0.01}_{-0.06}$	$13.64^{+1.54}_{-2.04}$	4.22	2.02	1.38	0.82

Errors are quoted at the 90% confidence level for 1 parameter of interest ($\Delta\chi^2 = 2.71$). Luminosity are absorption-corrected, while fluxes are corrected only for the Galactic absorption. Fe narrow-line energy fixed to $E_{rf} = 6.4$ keV, width fixed to 0 eV. † First line, intrinsic power law; second line, scattered power law. ‡ Parameters for the states tied in the fit. [a] In units of 10^{-4} photons keV^{-1} cm^{-2} s^{-1} @1 keV. [b] In units of 10^{22} cm^{-2}. [c] Ionization parameter $\xi \equiv 4\pi F_{ill}/n$ (erg cm s^{-1}), where F_{ill} is the ionizing flux and n is the hydrogen nucleus density (part cm^{-3}) of the illuminated slab. [d] Complement to one of the covered-to-uncovered flux ratio. [e] Line centroid energy, in keV. [f] Line width, in eV. [g] Ratio between the scattered flux and the partially-absorbed component.

7. Summary and discussion

We have presented a detailed spectral analysis of all the EPIC XMM-Newton data available for PG 1535+547. The source was observed first in November 2002, and then re-observed in January 2006; the latter data are presented here for the first time.

7.1. X-ray emission

Several features are clearly evident in the spectra of PG 1535+547 (see Fig. 2): a strong absorption between ∼0.7 and 2 keV, a spectral flattening at lower energies, a complex spectral shape in the iron band, and a drop in the emission at higher energies. Moreover, strong variations in shape and intensity are evident both on short and long timescales. The flux at energies <1 keV increases of a factor ∼10 in three years, then decreases by a factor ∼2 in six days. Above 3 keV the variability is significantly less important, with a change in flux by a factor ∼2 and ∼1.3 in the two time intervals, respectively.

We analyzed the three broadband (0.4−10 keV) EPIC spectra in the framework of two different models: an "absorption-based" scenario and a "relativistic reflection-based" one. In both cases, we detected a warm absorber, producing the strong absorption features observed in the 0.7−2 keV energy range. The spectral curvature observed at high energy can be reproduced either by a partial covering absorber or by a blurred relativistic reflection component. In both cases, we also detected a narrow Gaussian emission line, consistent with Kα fluorescence from almost neutral iron.

To account for the observed spectra assuming an accretion disk reflection contribution, the continuum emission must be intercepted by two layers of matter. The innermost, ionized absorber covers a high fraction (between ∼0.7 and ∼0.9) of the emission. The second layer, fully covering the source, is almost neutral ($\xi \sim 3.3$ erg cm s^{-1}). As noted, this model suggest a reflection produced in regions penetrating deeply toward the central black hole ($R_{in} < 2.50\ r_g$). The disk emissivity power-law index is close to 4, in agreement with theoretical expectations in the case of a small height for the primary source (e.g., Martocchia et al. 2002). The reflection fraction, defined as the ratio between the flux in the ionized reflection component and the total flux, is of the order of 50−60%, relatively large with respect to the 20−30% expected in the case of an isotropic illumination. The large amount of reflection from the disk observed in all states requires some mechanism to enhance the reflection component with respect to the intrinsic continuum, resulting in a strongly-suppressed intrinsic emission. Recent theoretical works, based on the "light bending" effect (Miniutti et al. 2003; Miniutti & Fabian 2004), or an inhomogeneous structure of the accretion disk due to violent clumping instabilities (Merloni et al. 2006), predict this kind of effect. A similar spectral behavior has been recently observed in the XMM-Newton spectra of Mrk 841 (Petrucci et al. 2007).

The main origin of the observed variability results in a change in the absorbers' properties (column densities and covering fractions), coupled with a change in the reflected component and the disk ionization state (see Table 5). The coverage of the inner absorber decreases, passing from November 2002 to (B) and (A) spectra. A higher disk reflection fraction and a higher coverage of the inner absorber explain the spectral changes observed passing from (A) to (B) states. The spectral index of the intrinsic continuum ($\Gamma \sim 2$) is consistent within the errors with the value found for radio-quiet AGN ($\Gamma \sim 1.9$; Piconcelli et al. 2005; Nandra et al. 2007) and the mean value found for other NLS1s in the 2−10 keV energy range ($\Gamma \sim 2.19$; Leighly 1999). The differences between November 2002 and January 2006 spectra imply stronger variations. The primary continuum changes both in shape (flatter in the oldest

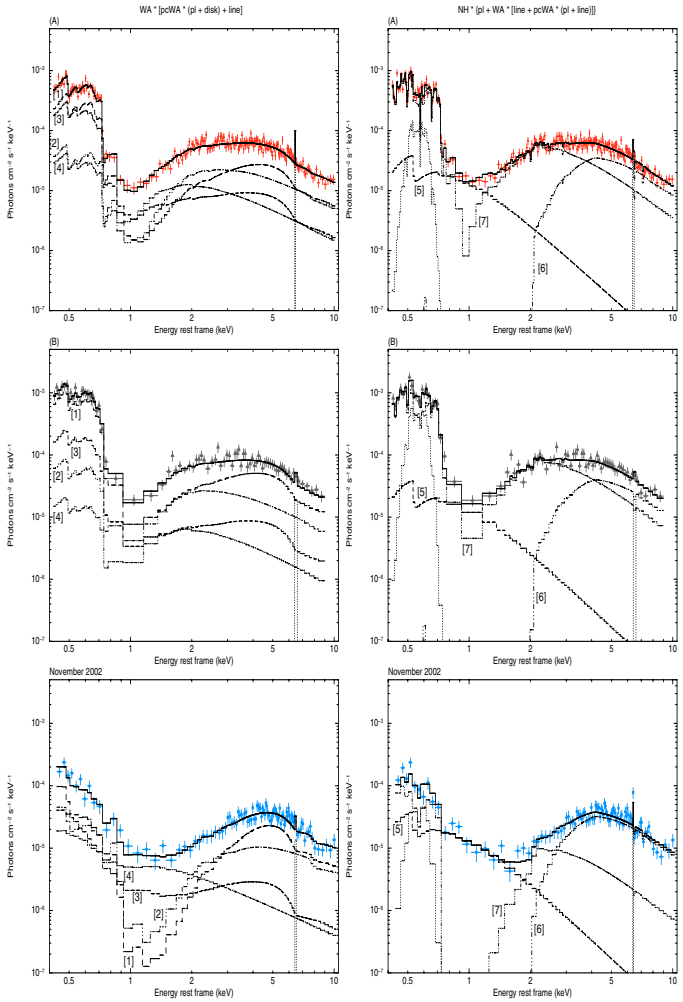

Fig. 5. Unfolded EPIC pn spectra of PG 1535+547 with the two adopted models fitted simultaneously to the three observations (see Sect. 6): the January 2006 (A) spectra (filled circles and red lines, *upper panels*) and (B) spectra (open triangles and gray lines, *middle panels*), and the November 2002 spectra (stars and sky-blue lines, *lower panels*). The solid lines correspond to the total best fit models. Over-plotted are the different components of each model: *left panels*, reflection from the disk (dashed line), power law (dash-dotted line), and narrow-emission line (dotted line), with the thickest lines identifying the fraction covered by the partial covering warm absorbed ([1] and [2] respectively), while the thinnest lines identify the fraction uncovered, ([3] and [4] respectively); *right panels*, scattered component (dashed line, [5]), absorbed power law (dash-dotted line) and emission lines (dotted line), with the thickest lines identifying the fraction covered by the partial covering warm absorber, [6], and the thinnest the fraction uncovered, [7].

observation, $\Gamma \sim 1.8$) and in intensity, and the accretion disk ionization state increases. The column densities of the two absorbers change in an opposite way: in November 2002 the column density of the inner absorber is higher ($N_{\rm H} \sim 2{\times}10^{23}$ cm^{-2}), while the outer absorber shows a column density lower than in the January 2006 spectra ($N_{\rm H} \sim 5 \times 10^{21}$ cm^{-2}).

Finally, a narrow Fe Kα emssion line is included in the model, probably produced by the obscuring torus postulated in AGN Unified Models (but other possible sites are the outer part of the accretion disk, or the optical BLR). Recently, a narrow emission line associated with cold iron was found to be almost ubiquitous in a sample of local radio-quiet Seyfert galaxies observed with XMM-Newton (Nandra et al. 2007). However, ~70% of these objects present further complexities in the iron band. Their spectral analysis shows that a model based on broad emission from an accretion disk is the best way to take this complexity into account. Jiménez-Bailón et al. (2005) noted that a narrow Fe Kα emission line is required in ~53% of the PG AGN sample studied by Piconcelli et al. (2005). The detection of broad relativistic lines is statistically significant in less than 10% of their sources (namely PG 0007+106, PG 0050+124, and PG 1116+215). Interestingly, their hard X-ray luminosity falls in the lower end of the range covered by the sample ($L_{2\text{-}10\,\rm keV} < 10^{44}$ erg s^{-1}): in the disk reflection framework, the unabsorbed 2−10 keV luminosity observed from PG 1535+547 changes from 9.7×10^{42} erg s^{-1} to 1.2×10^{43} erg s^{-1} and 7.2×10^{42} erg s^{-1} for the (A), (B) and November 2002 spectra, respectively. From their XMM-Newton data analysis of a large sample of AGN, Guainazzi et al. (2006) found that relativistically broadened Fe Kα lines are significantly more common in low luminosity ($L_{2\text{-}10\,\rm keV} \leq 10^{43}$ erg s^{-1}) AGN.

In the absorption-based scenario, several components are needed to properly reproduce the data: the primary power-law emission is partially covered by the above mentioned warm absorber, and totally covered by a second ionized absorber. A soft scattered component is also present. In addition to the Fe Kα line, an O VII emission line (not required in the reflection-based model) is also detected at $E \sim 0.57$ keV. Finally, the whole emission is absorbed by a rather low (~2×10^{21} cm^{-2}) column density of neutral gas.

We account for the observed variability by variations of the two warm absorber components. Between November 2002 and January 2006 observations, the covering fraction of the inner absorber decreased significantly (passing from ~0.9 to ~0.55), leading to a different shape of the complex curvature seen at high energies. In the meantime, the ionization state of the outer absorber increased (from ~60 to ~90 erg cm s^{-1}) in a manner roughly proportional to the increase in unabsorbed luminosity. This may suggest that the density and location of the warm absorber has not changed in this lapse of time. Instead, the differences observed between (A) and (B) spectra can be explained by a variation of the covering fraction of the inner, ionized absorber.

The inner, partially-covering warm absorber presents a lower ($\xi \sim 20$ erg cm s^{-1}) ionization state than the fully covering warm absorber. In theoretical models of accretion disk winds (e.g., Proga & Kallman 2004), two phases of ionized gas are predicted to coexhist in the inner regions of accretion disks, where the wind is "launched". In particular, the wind itself is shielded from the central ionizing source by a higher ionization component. In this framework, it is possible that we are looking PG 1535+547 at the base of the wind, with the partial covering absorber corresponding to the "wind blobs" and the totally covering absorber corresponding to the highly-ionized shielding phase. The latter warm absorber component may be responsible for the scattering of the primary emission into our line of sight. The very small scattering fraction (few parts per thousand) could thus be explained by the low column density (~4×10^{22} cm^{-2}) of the scatterer, coupled with a possible anisotropic distribution around the source. In this scenario, the emission line at ~6.4 keV can be produced by transmission through the high column density, partially-covering absorber, while the line detected at ~0.6 keV could be associated to photoionized emission occurring in the low column density, totally covering absorber. The presence of unresolved photoionized emission lines would then naturally explain the steepening of the scattered power law with respect to the intrinsic one. The primary power-law emission is somewhat steep ($\Gamma \sim 2.5$), but consistent within the errors with the values found by Leighly (1999). Finally, the small ($N_{\rm H} \sim 2{\times}10^{21}$ cm^{-2})

neutral column density absorbing the whole emission and affecting only the data below 0.5 keV could be ascribed either to dust lanes in the host galaxy or to the presence of dust in the wind and/or scattering region. Overall, the complex spectra of PG 1535+547 seem, thus, fully compatible with the presence of a strong and complex ionized outflow along the line of sight.

7.2. The broad-band SED of PG 1535+547

Considering the strong variability observed in the X-ray band, it is interesting to look at the multiwavelength emission properties of PG 1535+547. In the UV band, Gallagher et al. (2001) noted a variation of 30% between the *IUE* data of November 1982 and May 1984, and earlier *IUE* observation from June 1982 and September 1982, which are consistent with later *HST* spectra. The fluxes observed by the OM simultaneously to the new EPIC spectra presented here are in good agreement with the *HST* data.

At long wavelengths, PG 1535+547 is the only radio-quiet AGN observed by Neugebauer & Matthews (1999) where a variation in the near-infrared (NIR) emission from 1980 to 1998 is reported: in particular, the flux in 4 bands from 1.27μm to 3.7μm rises 0.5 mag between 1993 and 1996, going back to the previous value between 1996 and 1998. The continuum emission observed in Seyfert galaxies at $\lambda \gtrsim 2\ \mu$m is very likely dominated by thermal radiation from the inner edge of the dust torus (e.g., Kobayashi et al. 1993), heated by the radiation originated in the central active nucleus (Haas et al. 2003). How much the torus extends toward the black hole depends on the irradiating luminosity and on the dust composition, that determine the distance at which the temperature is so high that the dust begins to sublimate. So, the dust evaporation radius can be estimated from the bolometric luminosity, $R_{\rm evap} \simeq 0.06\sqrt{L_{\rm bol}/(10^{45}{\rm erg\ s^{-1}})}$ pc (Netzer & Laor 1993; Hill et al. 1996). Assuming that the inner radius of the torus roughly corresponds to $R_{\rm evap}$, and adopting the bolometric luminosity estimated from the [O III] line width by Zhang & Wang (2006), $L_{\rm bol} \sim 1.4{\times}10^{45}$ erg s^{-1}, we can estimate the dimension of the region producing the observed NIR emission, $R_{\rm torus} \sim 0.07$ pc. The minimum timescale for an observable variability implied by $R_{\rm torus}$ is of the order of a year. Therefore, it is consistent with the possibility that the observed NIR variability is the reaction of the torus to the long timescale X-ray variable emission.

In Sect. 2, we have mentioned the high-optical continuum polarization demonstrated by PG 1535+547, $P = 2.5\%$ (Berriman et al. 1990). The optical polarization spectrum presented by Smith et al. (1997) exhibits a rise in the linear polarization P toward shorter wavelength (roughly proportional to λ^{-1}), which continues into the UV band down to 2000 Å. A complex behavior of the polarization position angle across the Hα feature is also observed. To explain the continuum and line polarizations, the authors suggest the presence of different scattering regions, with at least part of the scattering material intermixed with the line-emitting gas. Warm electrons responsible for the observed polarization in the emission-line wings (i.e., the interaction with the warm absorber required by the X-ray observations) would be a possible alternative. Considering the two-component scattering geometries recently proposed to account for the polarization properties of all Seyfert galaxies simultaneously (Smith 2002, 2004), it is possible that we are observing PG 1535+547 at a "privileged" angle. Although the available information does not allow Smith et al. (2004) to confidently assign a polarization class ("polar-" or "equatorially-" scattered Seyfert) to this object, it is possible that our line of sight passes very close to the absorbing torus. This seems to be a coherent scenario that takes into account observations in different bands; further multiwavelength observations are required to test this hypothesis.

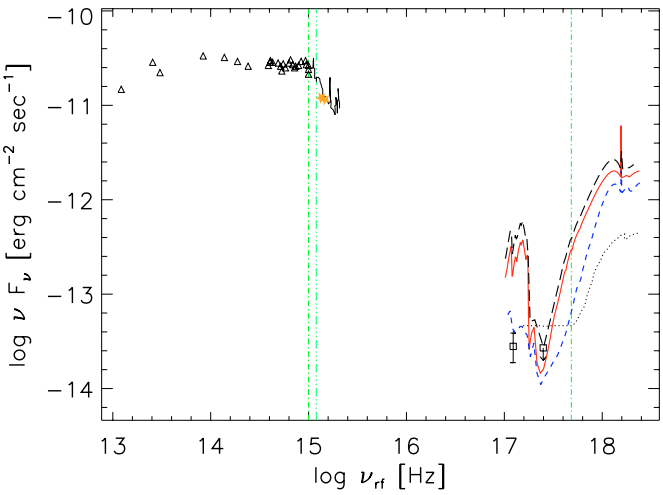

Fig. 6. Spectral energy distribution for PG 1535+547. At low frequencies, open triangles are infrared and optical continuum data from Neugebauer et al. (1987), and the thin solid curve is the UV spectrum from *HST* (Gallagher et al. 2001). Yellow-filled stars indicate the XMM-Newton OM fluxes observed in January 2006. In the X-ray energy range, *ROSAT* data point and upper limit are marked with open squares, while the black-dotted line indicates the *ASCA* best fitting model (Gallagher et al. 2001). The three observed XMM-Newton EPIC fluxes are shown with the black long-dashed line, January 2006 spectrum (B); red-solid line, January 2006 spectrum (A); blue-dashed line, November 2002 spectrum. The vertical thin dot-dashed light-green lines correspond to $\lambda_{\rm rf} = 3000$ Å and $E_{\rm rf} = 2$ keV, while the green dot-dot-dot-dashed line corresponds to $\lambda_{\rm rf} = 2500$ Å.

In Fig. 6, we present the broadband SED of PG 1535+547. A stronger high-energy variability than at low frequencies is clearly evident. The light-green, dot-dashed lines correspond to $\lambda = 3000$ Å and $E = 2$ keV in the source rest frame, i.e., where the low- and high-energy fluxes used by Brandt et al. (2000) to evaluate the $\alpha_{\rm ox}$ are calculated. The change observed in the X-ray flux in front of a roughly constant UV flux implies a variability in the X-ray-to-optical index even higher than previously reported: Gallagher et al. (2001) estimated for *ROSAT* and *ASCA* observations $\alpha_{\rm ox} < -2.17$ and $\alpha_{\rm ox} = -2.03$. The *observed* indices measured from the new XMM-Newton spectra are considerably higher: we can compute the optical fluxes rescaling the UV *HST* spectrum to the OM data (that, we stress, are simultaneous to the X-ray fluxes), obtaining $\alpha_{\rm ox} = -1.66$ and -1.65 for the (A) and (B) spectra. This result implies a change in the classification of PG 1535+547 as X-ray weak source.

Many authors have investigated the relation between rest-frame UV and soft X-ray AGN emission, and its dependence with redshift and/or optical luminosity. Most studies have concluded that there is no evidence for a redshift dependence, while the X-ray emission is correlated with the UV emission, and the ratio of the monochromatic X-ray and UV luminosities, $\alpha_{\rm ox}$, decreases as the UV emission increases (e.g., Vignali et al. 2003; Strateva et al. 2005; Steffen et al. 2006; Just et al. 2007). In particular, Strateva et al. (2005) combined radio quiet sources from the SDSS, a heterogeneous low-redshift Seyfert 1 sample, and a heterogeneous high-redshift sample. Performing their analysis both with and without the Seyfert 1 sample, they

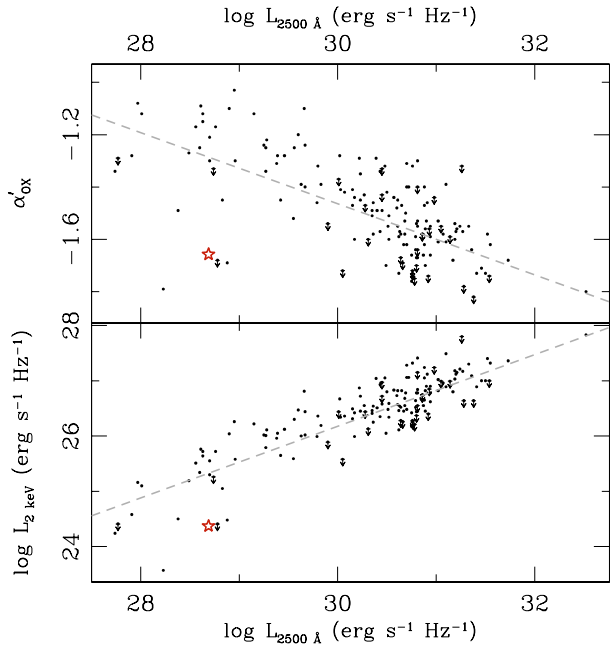

Fig. 7. Dependence on the 2500 Å monochromatic luminosity of α'_{ox} (*upper panel*) and $L_{2\,keV}$ (*lower panel*). Black-filled circles mark data from Strateva et al. (2005) for their "main" *SDSS* sample (155 objects with $0.1 \lesssim z \lesssim 4.5$); arrows indicate upper limits in the X-ray detection. Dashed lines are the best–fit linear relations for their combined sample ("main" *SDSS* sample + high-redshift sample + Seyfert 1 sample): $\alpha'_{ox} = -0.136 \cdot \log L_{2500\,Å} + 2.616$ (*upper panel*) and $\log L_{2\,keV} = 0.648 \cdot \log L_{2500\,Å} + 6.734$ (*lower panel*). Red open-star marks the position of PG 1535+547 as observed in January 2006 (to avoid confusion we report only the values from the (A) data, being the two states indistinguishable).

found that the monochromatic luminosities at 2500 Å and 2 keV are correlated (with a slope lower than 1). The broadband spectral index, calculated here at $\lambda = 2500$ Å, $\alpha'_{ox} \equiv \log(F_{2\,keV}/F_{2500\,Å})/\log(\nu_{2\,keV}/\nu_{2500\,Å})$, is anticorrelated with the rest-frame monochromatic UV luminosity. The January 2006 XMM-Newton observations put PG 1535+547 outside both relations (see Fig. 7). From the observed luminosity at 2 keV, we would expect a spectral index[14] $\alpha'_{ox} \sim -1.09$, while the UV luminosity obtained from the OM data would imply an index $\alpha'_{ox} \sim -1.29$. Both values differ considerably from the observed indices, $\alpha'_{ox} = -1.66$ and -1.67 for the (A) and (B) spectra, respectively. These numbers should be taken with caution: the host-galaxy contribution was not excluded from the January 2006 OM data, thus the nuclear UV flux could be lower than the value estimated here. However, taking this consideration into account, PG 1535+547 appears to be still underluminous in the X-ray band if compared with optically-selected sources in the same bin of UV luminosity[15], a property shown by other NLS1s with high-energy spectral complexity (e.g., Gallo 2006).

[14] The expected luminosities at 2500 Å for the (A) and (B) spectra are $L_{2500\,Å} = 1.65 \times 10^{27}$ and 2×10^{27} erg s^{-1} Hz^{-1}, respectively.

[15] From Fig. 10 in Strateva et al. (2005), only 1 of 37 Seyfert 1 falls in this bin of α'_{ox} (*upper panel*), while in their main SDSS sample they have only 1 AGN with $L_{2500\,Å} < 3.16 \times 10^{30}$ erg s^{-1} Hz^{-1} with $-1.7 < \alpha'_{ox} < -1.6$ (compared with 16 sources with $L_{2500\,Å} > 3.16 \times 10^{30}$ erg s^{-1} Hz^{-1}, *lower panel*).

8. Conclusions

PG 1535+547 is a bright Narrow Line Seyfert 1 galaxy, whose high-energy emission shows strong variability both in shape and flux. In this paper, we have reported a consistent analysis of the three available XMM-Newton datasets of this object; the observations taken in January 2006 are presented here for the first time. The availability of high-quality data obtained at different epochs with the same satellite opened us up to the very intriguing possibility of studying in detail the complex emission of PG 1535+547, the origin of the spectral features as well as of the strong variability observed. The main aspects of this work can be summarized as follows.

1 Strong flux and spectral variability is observed on timescales of years and shorter; the strongest variation is observed in the soft X-ray band, at energies lower than 3 keV. The importance of absorption structures is evident in all the states, a result consistent with the strong polarization continuum and the absorption features observed in the optical-UV.
2 The broadband (0.4–10 keV) EPIC spectra can be described well either assuming an intrinsic continuum and reflection from an accretion disk covered by a system of ionized-absorbing materials (the "reflection-based" model), or by an intrinsic continuum and a scattered component, with a complex combination of neutral-absorbing material and a two-phase warm absorber covering the central source in different ways (the "absorption-based" model). In the former case, the XMM-Newton observations imply evidence of important reprocessing from the disk of the intrinsic continuum (in terms of relativistically blurred reflection component and broad iron line) for all the three states.
3 In both scenarios, the analysis suggests that the observed variability can be ascribed mainly to changes in the absorbers, although in the former the ionization of the emitting region of the disk plays a role, too. Further, deeper observations are needed to model correctly the continuum in the 4–7 keV range and better constrain the parameters of the broad line and/or the absorbing structures, a task made particularly difficult by the well-known interplay between absorbers and broad features in the resulting spectrum. Moreover, a spectral coverage extended at higher energy would be able to fix with higher accuracy the intrinsic spectral index and the contribution from the reflection.
4 Finally, unrelated X-ray and optical variabilities imply a *change in the classification of PG 1535+547 as X-ray weak source*. The classification of a source as X-ray weak AGN seems to depend strongly on the date of the high-energy observations; the suggestion is that a similar behavior can also occur for other sources in intermediate range $-2 < \alpha_{ox} < -1.7$. The nature of these sources as a homogeneous class is not so clear, as they include objects like PHL 1811, which seems to be intrinsically X-ray weak (Leighly et al. 2007a,b), and PG 2112+059, for which the weakness and the X-ray variability are ascribed to change in the intrinsic continuum instead of to absorption effects (Schartel et al. 2007).

To conclude, whatever model used, the changes observed in the emission of PG 1535+547 imply physical variations occurring in regions close to the central black hole. Moreover, α_{ox} is definitely a variable parameter (see also Gallo 2006; Grupe et al. 2006): it seems that some sources go through phases where they appear to be X-ray weak and for most of them the X-ray weakness is a temporary event. Further investigations of their

high-energy emission with a simultaneous multiwavelength coverage are needed.

Acknowledgements. We warmly thank the referee, Dr. Grupe, for his suggestions that significantly improved the paper. We are grateful to T. Kallman, C. Gordon, and K. A. Arnaud for enlightening discussions regarding XSTAR and XSPEC interplay. LB thanks L. Maraschi and V. Braito for useful discussions. MG would like to thank G. Ponti, M. Dadina, and G. Palumbo for key and pleasant discussions. M.C., M.G., and C.V. acknowledge finantial support from ASI contract number ASI/INAF I/023/05/0. Based on observations obtained with XMM-Newton (an ESA science mission with instruments and contributions directly funded by ESA Member States and the USA, NASA).

References

Arnaud, K. A. 1996, in Astronomical Data Analysis Software and Systems V, ASP Conf. Ser., 101, ed. G. H. Jacoby, & J. Barnes, 17
Ashton, C. E., Page, M. J., Blustin, A. J., et al. 2004, MNRAS, 355, 73
Berriman, G., Schmidt, G. D., West, S. C., & Stockman, H. S. 1990, ApJS, 74, 869
Blustin, A. J., Page, M. J., Fuerst, S. V., Branduardi-Raymont, G., & Ashton, C. E. 2005, A&A, 431, 111
Boller, T., Balestra, I., & Kollatschny, W. 2007, A&A, 465, 87
Boroson, T. A. 2002, ApJ, 565, 78
Boroson, T. A., & Green, R. F. 1992, ApJS, 80, 109
Brandt, W. N., Laor, A., & Wills, B. J. 2000, ApJ, 528, 637
Brinkmann, W., Grupe, D., Branduardi-Raymont, G., & Ferrero, E. 2003, A&A, 398, 81
Brinkmann, W., Papadakis, I. E., & Ferrero, E. 2004, A&A, 414, 107
Cappi, M. 2006, Astron. Nachr., 327, 1012
Carini, M. T., Noble, J. C., Taylor, R., & Culler, R. 2007, AJ, 133, 303
Chevallier, L., Collin, S., Dumont, A.-M., et al. 2006, A&A, 449, 493
Costantini, E., Kaastra, J. S., Arav, N., et al. 2007, A&A, 461, 121
Crummy, J., Fabian, A. C., Gallo, L., & Ross, R. R. 2006, MNRAS, 365, 1067
De Vaucouleurs, G., De Vaucouleurs, A., Corwin Jr., H. G., et al. 1991 (New York: Springer-Verlag)
de Veny, J. B., & Lynds, C. R. 1969, PASP, 81, 535
den Herder, J. W., Brinkman, A. C., Kahn, S. M., et al. 2001, A&A, 365, L7
Ehle, M., Breitfellner, M., Dahlem, M., et al. 2001, XMM-Newton Users' Handbook Issue 2.0 http://xmm.vilspa.esa.es/external/xmm_user_support/documentation/uhb_2.0/index.html
Fabian, A. C., Vaughan, S., Nandra, K., et al. 2002, MNRAS, 335, L1
Gallagher, S. C., Brandt, W. N., Laor, A., et al. 2001, ApJ, 546, 795
Gallo, L. C. 2006, MNRAS, 368, 479
Gierliński, M., & Done, C. 2004, MNRAS, 349, L7
Gierliński, M., & Done, C. 2006, MNRAS, 371, L16
Grupe, D., & Mathur, S. 2004, ApJ, 606, L41
Grupe, D., Beuerman, K., Mannheim, K., et al. 1995, A&A, 300, L21
Grupe, D., Mathur, S., & Komossa, S. 2004a, AJ, 127, 3161
Grupe, D., Wills, B. J., Leighly, K. M., & Meusinger, H. 2004b, AJ, 127, 156
Grupe, D., Leighly, K. M., Komossa, S., et al. 2006, AJ, 132, 1189
Grupe, D., Komossa, S., & Gallo, L. C. 2007, ApJ, 668, L111
Guainazzi, M., & Bianchi, S. 2007, MNRAS, 374, 1290
Guainazzi, M., Bianchi, S., & Dovčiak, M. 2006, Astron. Nachr., 327, 1032
Haas, M., Klaas, U., Müller, S. A. H., et al. 2003, A&A, 402, 87
Halpern, J. P. 1984, ApJ, 281, 90
Hill, G. J., Goodrich, R. W., & Depoy, D. L. 1996, ApJ, 462, 163
Immler, S., Brandt, W. N., Vignali, C., et al. 2003, AJ, 126, 153
Jiménez-Bailón, E., Piconcelli, E., Guainazzi, M., et al. 2005, A&A, 435, 449
Just, D. W., Brandt, W. N., Shemmer, O., et al. 2007, ApJ, 665, 1004
Kallman, T., & Bautista, M. 2001, ApJS, 133, 221
Kellermann, K. I., Sramek, R., Schmidt, M., Shaffer, D. B., & Green, R. 1989, AJ, 98, 1195
Kobayashi, Y., Sato, S., Yamashita, T., Shiba, H., & Takami, H. 1993, ApJ, 404, 94
Laor, A. 1991, ApJ, 376, 90
Laor, A., Fiore, F., Elvis, M., Wilkes, B. J., & McDowell, J. C. 1997, ApJ, 477, 93
Leighly, K. M. 1999, ApJS, 125, 317
Leighly, K. M., Halpern, J. P., Jenkins, E. B., & Casebeer, D. 2007a, ApJS, 173, 1
Leighly, K. M., Halpern, J. P., Jenkins, E. B., et al. 2007b, ApJ, 663, 103
Magdziarz, P., & Zdziarski, A. A. 1995, MNRAS, 273, 837
Martocchia, A., Matt, G., & Karas, V. 2002, A&A, 383, L23
Mathur, S., & Grupe, D. 2005, A&A, 432, 463
McKernan, B., Yaqoob, T., & Reynolds, C. S. 2007, MNRAS, 379, 1359
Merloni, A., Malzac, J., Fabian, A. C., & Ross, R. R. 2006, MNRAS, 370, 1699
Miller, L., Turner, T. J., Reeves, J. N., et al. 2006, A&A, 453, L13
Miniutti, G., & Fabian, A. C. 2004, MNRAS, 349, 1435
Miniutti, G., Fabian, A. C., Goyder, R., & Lasenby, A. N. 2003, MNRAS, 344, L22
Murphy, E. M., Lockman, F. J., Laor, A., & Elvis, M. 1996, ApJS, 105, 369
Nandra, K., O'Neill, P. M., George, I. M., & Reeves, J. N. 2007, MNRAS, 942
Narayanan, D., Hamann, F., Barlow, T., et al. 2004, ApJ, 601, 715
Netzer, H., & Laor, A. 1993, ApJ, 404, L51
Neugebauer, G., & Matthews, K. 1999, AJ, 118, 35
Neugebauer, G., Green, R. F., Matthews, K., et al. 1987, ApJS, 63, 615
Nicastro, F., Fiore, F., & Matt, G. 1999, ApJ, 517, 108
Osterbrock, D. E., & Pogge, R. W. 1987, ApJ, 323, 108
Petrucci, P. O., Ponti, G., Matt, G., et al. 2007, A&A, 470, 889
Phillips, M. M. 1978, ApJS, 38, 187
Piconcelli, E., Jimenez-Bailón, E., Guainazzi, M., et al. 2004, MNRAS, 351, 161
Piconcelli, E., Jimenez-Bailón, E., Guainazzi, M., et al. 2005, A&A, 432, 15
Proga, D., & Kallman, T. R. 2004, ApJ, 616, 688
Protassov, R., van Dyk, D. A., Connors, A., Kashyap, V. L., & Siemiginowska, A. 2002, ApJ, 571, 545
Reynolds, C. S., & Nowak, M. A. 2003, Phys. Rep., 377, 389
Risaliti, G., Elvis, M., Gilli, R., & Salvati, M. 2003, ApJ, 587, L9
Ross, R. R., & Fabian, A. C. 2005, MNRAS, 358, 211
Ross, R. R., Fabian, A. C., & Young, A. J. 1999, MNRAS, 306, 461
Schartel, N., Rodríguez-Pascual, P. M., Santos-Lleó, M., et al. 2007, A&A, 474, 431
Schartel, N., Rodríguez-Pascual, P. M., Santos-Lleó, M., et al. 2005, A&A, 433, 455
Schmidt, M., & Green, R. F. 1983, ApJ, 269, 352
Schurch, N. J., & Done, C. 2006, MNRAS, 371, 81
Shuder, J. M., & Osterbrock, D. E. 1981, ApJ, 250, 55
Smith, P. S., Schmidt, G. D., Allen, R. G., & Hines, D. C. 1997, ApJ, 488, 202
Sobolewska, M. A., & Done, C. 2007, MNRAS, 374, 150
Steffen, A. T., Strateva, I., Brandt, W. N., et al. 2006, AJ, 131, 2826
Strateva, I. V., Brandt, W. N., Schneider, D. P., Vanden Berk, D. G., & Vignali, C. 2005, AJ, 130, 387
Strüder, L., Briel, U., Dennerl, K., et al. 2001, A&A, 365, L18
Sulentic, J. W., Zwitter, T., Marziani, P., & Dultzin-Hacyan, D. 2000, ApJ, 536, L5
Sulentic, J. W., Dultzin-Hacyan, D., Marziani, P., et al. 2006, Rev. Mex. Astron. Astrofis., 42, 23
Tremaine, S., Gebhardt, K., Bender, R., et al. 2002, ApJ, 574, 740
Turner, M. J. L., Abbey, A., Arnaud, M., et al. 2001, A&A, 365, L27
Véron-Cetty, M.-P., Véron, P., & Gonçalves, A. C. 2001, A&A, 372, 730
Vestergaard, M., & Peterson, B. M. 2006, ApJ, 641, 689
Vignali, C., Brandt, W. N., & Schneider, D. P. 2003, AJ, 125, 433
Weymann, R. J., Morris, S. L., Foltz, C. B., & Hewett, P. C. 1991, ApJ, 373, 23
Zdziarski, A. A., Johnson, W. N., Done, C., Smith, D., & McNaron-Brown, K. 1995, ApJ, 438, L63
Zhang, E.-P., & Wang, J.-M. 2006, ApJ, 653, 137
Zhou, X.-L., Yang, F., Lu, X.-R., & Wang, J.-M. 2007, AJ, 133, 432